Moored observations of mesoscale features in the Cape Basin: Characteristics and local impacts on water mass distributions

Marion Kersalé[1,2], Tarron Lamont[1,3], Sabrina Speich[4], Thierry Terre[5], Remi Laxenaire[4], Mike J. Roberts[3,6], Marcel A. van den Berg[3] and Isabelle J. Ansorge[1]

[1]Marine Research Institute, Department of Oceanography - University of Cape Town, Rondebosch, South Africa
[2]Cooperative Institute for Marine and Atmospheric Studies, University of Miami, and NOAA/Atlantic Oceanographic and Meteorological Laboratory, Miami, Florida
[3]Oceans and Coastal Research, Department of Environmental Affairs, South Africa
[4]Laboratoire de Météorologie Dynamique, UMR 8539 École Polytechnique, ENS, CNRS, Paris, France
[5]IFREMER, Univ. Brest, CNRS, IRD, Laboratoire d'Océanographie Physique et Spatiale (LOPS), IUEM, Plouzané, France
[6]Ocean Science & Marine Food Security, Nelson Mandela University, Port Elizabeth, South Africa

Correspondence to: Marion Kersalé (marion.kersale@noaa.gov)

Abstract. The eastern side of the SAMBA array (South Atlantic Meridional overturning circulation Basin-wide Array) along the latitude 34.5°S is used to assess the nonlinear, mesoscale dynamics of the Cape Basin. This array presently consists of current meter moorings and CPIES (bottom mounted Inverted Echo Sounders with pressure sensor and current meter) deployed across the continental slope. These data, available from September 2014 to December 2015, combined with satellite altimetry allow us to investigate the characteristics and the impact of these mesoscale structures on local water masses distribution and cross-validate the different data sets. We demonstrate that the upper slope moorings are affected by cyclonic eddies generated at the South Benguela upwelling front, while the deeper slope moorings are affected by the more complex dynamics of the Cape Basin involving Agulhas Rings and cyclonic eddies. This complex dynamics induces strong intra-seasonal upper-ocean velocity variations and water masses exchanges across the shelf and the open ocean, but also across the subantarctic and subtropical waters. Under four case studies, the full-water column hydrographic properties of each mesoscale feature has been evaluated. Our analyses show that exchange of water masses happens through the advection of water by mesoscale eddies but also via wide water mass intrusions engendered by the existence of intense dipoles. The high spatial and temporal scales resolved by the moorings allows us to define the substantial role of these mesoscale features over the full-water column. Future investigations with longer time series at these existing sites will lead to a better understanding of the eastern boundary current variability, and ultimately improve our understanding of the strength and variability of the Meridional Overturning Circulation.

Ocean Science
Discussions

1 Introduction

35 The Meridional Overturning Circulation (MOC) is a three-dimensional circulation pattern encompassing all ocean basins. The MOC is the key link in the global transport of mass and heat and has profound impacts on regional and global climates (*e.g.,* Rahmstorf, 2015). While the MOC has often been described through simple schematics (the Global Conveyor Belt of Gordon (1986) and Broeker (1991)), or, in models, in terms of a meridional mean stream-function (*e.g.,* Bingham et al., 2007), it has, in reality, a very complex nature that is slowly becoming better understood (*e.g.,* Lozier, 2010).

40 The overturning circulation and horizontal fluxes of heat and freshwater in the Atlantic Ocean are fundamental controls on the MOC. Cold and salty North Atlantic Deep Water (NADW) flows southward along the eastern coast of America and through the basin interior, compensated by a northward flow that is a mixture of warm/salty surface waters and cooler/fresher Antarctic Intermediate Waters (AAIW) (*e.g.,* Gordon et al., 1992). Recognition the Atlantic's critical role led to long-term observations of the Atlantic MOC (AMOC), and the creation of the first trans-basin AMOC array at 26.5ºN -

45 the RAPID/MOCHA/WBTS array (Baringer and Larson, 2001; Cunningham et al., 2007; Kanzow et al. 2007, Meinen and Garzoli, 2014; McCarthy et al., 2015; Srokosz and Bryden, 2015). Other long-term observing systems measuring components of AMOC have been deployed at different latitudes in the Atlantic, (39°N: Peña-Molino et al. (2012); 37°N: Rossby et al. (2010); 16°N - Meridional Overturning Variability Experiment – MOVE: Send et al. (2011); 11°S: Schott et al. (2005) and Hummels et al. (2015)). Some of these observations have been used to examine the meridional coherence or

50 connectivity of AMOC (*e.g.,* Elipot et al. 2017), and to assess the temporal variability of the AMOC.
Numerical models suggest that a large source of AMOC variability originates in the South Atlantic via transformations and mixing inducing changes in the thermohaline characteristics of water masses and via inter-basin heat and fresh water fluxes from the Pacific and Indian Oceans into the Atlantic (Weijer et al., 1999; Biastoch et al., 2008). The need for AMOC observations in the subtropical South Atlantic, led to the establishment of the South Atlantic MOC (SAMOC) initiative to

55 enhance further AMOC observing systems in this area (Garzoli and Matano, 2011). As part of SAMOC, several efforts to document the inflows of the two main paths of the upper limb of the AMOC have been undertaken across the Drake Passage (*e.g.,* Chereskin et al., 2009) and south of South Africa (*e. g.,* GoodHope line - Ansorge et al., 2005; Gladyshev et al., 2008; Speich et al. 2007). A trans-basin AMOC array, which began as a pilot array in 2008-2009 (Speich et al. 2010; Meinen et al., 2013), continues to grow along 34.5°S, a crucial latitude to evaluate the MOC variability and the impact of inter-ocean

60 exchanges (Perez et al., 2011; Schiermeier, 2013). The South Atlantic MOC Basin-wide Array (SAMBA) is a collaboration between Argentina, Brazil, France, South Africa and the United States, with moorings located on the western and eastern boundaries (Speich et al., 2010; Meinen et al., 2013; Ansorge et al., 2014). Since the pilot deployment described in Meinen et al. (2013), the number of moorings on the boundaries has increased dramatically. The western boundary buoyancy anomalies have been well studied (e.g., Meinen et al., 2012, Meinen et al., 2017; Valla et al., under review, 2017) but the

65 eastern boundary anomalies have not yet been examined along 34.5°S. Focusing on the eastern margin (Figure 1 shows the easternmost SAMBA moorings), the transport of warm and salty Indian Ocean waters into the Atlantic Ocean through the

Cape Basin—the Agulhas leakage (*e.g.*, Gordon et al., 1992; de Ruijter et al., 1999) — injects buoyancy anomalies that impact the AMOC strength with a clear implication for climate studies (Beal et al., 2011). The Agulhas leakage is controlled by nonlinear, mesoscale dynamics mainly through the shedding of large Agulhas rings, eddies, and filaments from the

70   Agulhas current and its Retroflection (Lutjeharms and Cooper, 1996; de Ruijter et al., 1999; Lutjeharms, 2006).

These former studies have first lead to a quantification of energy, heat and salt fluxes of these features (*e.g.*, de Ruijter et al., 1999, and references therein). The first inter-ocean exchange estimates were based on individual hydrographic cruise data combined with altimetric tracking of Agulhas rings (Olson, 1986; Gordon and Haxby, 1990; Duncombe Rae, 1991; van Ballegooyen et al., 1994; Byrne et al., 1995). These combined data revealed the presence of 4 to 8 rings per year propagating

75   into the South Atlantic with speeds ranging between 5 and 10 km day^{-1}, with a diameter up to 400 km and a depth impact between 600 and 1100 m. The associated inter-ocean volume transport per ring was estimated between 0.5 and 3 Sv (1 Sv=10^6 m^3 s^{-1}). These first estimates, based on altimetric statistics and individual ring observations, led to a large range of volume fluxes.

Understanding the Cape Basin circulation is crucial for many studies, at large scales for global thermohaline circulation and

80   at regional scales for water mass distribution, local dynamics, ecosystem assessments and air-sea interactions. As part of international and national programmes (SAMOC and SANAP - South African National Antarctic Programme) repeat monitoring lines attached to relief voyages of South African scientific bases have been conducted. In the framework of these projects, our work focuses on the eastern part of the SAMBA array offering an ideal set of data to observe mesoscale dynamics—a key link between Indian and Atlantic water exchanges (Figure 1). The analysis of the SAMBA-east moored

85   data sets, from September 2014 to December 2015, provides some accurate information on the mesoscale features in the Cape Basin. The main focus of this study is to characterize these mesoscale structures and quantify their local impact on water mass distribution from different data sets obtained along the SAMBA array. Understanding the characteristics of the local dynamics associated with the Greater Agulhas Current system represents a fundamental step towards our understanding of the strength and variability of the AMOC and of the Earth climate system variability.

90   **2 Data and Methods**

This study was conducted within the framework of the SAMOC project, one of the aims of which is maintaining a trans-basin mooring line along 34.5°S. Focusing on the eastern part of the SAMBA array, this observing system presently consists of four "tall" current meter moorings (hereafter tall-moorings), eight CPIES (Current and Pressure Inverted Echo Sounders) and two bottom mounted ADCP (Acoustic Doppler Current Profiler) moorings that are deployed from the shelf to near the

95   Walvis Ridge offshore. In this study, we will focus on the 4 tall-moorings (hereafter named M1, M2, M3 and M4) extending from the continental shelf edge, at 1121 m of depth, to 15°E, at 4474 m of depth, deployed in September 2014, by the Department of Environmental Affairs (DEA) and the University of Cape Town (UCT), South Africa from the RV *Algoa*, and

the CPIES nearest to them (hereafter named C1, C2, C3 and C4), deployed in September 2013, by IFREMER, France and DEA, South Africa from the RV *SA Agulhas II* (Figure 1, Table I).

100 The characteristics of the moorings and CPIES used in this study are summarized in Table I. All tall-moorings (M1-M4) have a sub-surface depth of 500 m, with an upward looking 75kHz RDI ADCP deployed in uppermost float, set to sample the top 500 m of the water column. At selected depths along the mooring lines, SBE 37 MicroCat's, a high-accuracy conductivity and temperature recorder with optical oxygen sensors were attached. All instruments (ADCP and SBE Microcat's) were still recording on recovery, except for two SBE37 MicroCat's. These two units were both from M4, fixed at

105 1340 m and 3985 m depths respectively. Both instruments stopped recording, in November 2014, due to low battery power. The sampling period was 1h. The collected data were tidally filtered using a second-order Butterworth filter with a 3 days cut-off period. CPIES recorded hourly measurements of round-trip acoustic travel time, bottom pressure, and the velocity at 50 m above the sea-floor. All the CPIES have been recovered and re-deployed except C3 which was unfortunately destroyed and lost. After removing the linear drift associated with the pressure sensor (following Meinen et al., 2013), the same tidal

110 filter has been applied on the CPIES data. The CPIES records were sub-sampled to one value per day at noon UTC. We will primarily look at results from the dynamic height moorings (Sections 3.2 and 3.3), and secondarily look at CPIES (Section 3.5).

Hydrographic sampling has been conducted along the eastern section of the SAMBA transect during various cruises on board the RV *SA Agulhas II* (September 2013, September 2014, and July 2015) and the RV *Algoa* (September 2014, and

115 December 2015). During each cruise, Conductivity-Temperature-Depth (CTD) casts were conducted at several stations along the transect, measuring temperature, salinity and density using multiple SeaBird Electronics SBE 911+ CTD systems and sensors. CTDs were conducted from the surface to within 5-10 m of the sea floor on the RV *SA Agulhas II*, while CTDs on the RV *Algoa* were conducted to a maximum depth of 1000 m. Discrete seawater samples were collected at selected depths for analysis of salinity with a Guildline Portsal salinometer and used for calibration of the CTD conductivity sensors (van

120 den Berg, 2015). Vertical profiles of temperature and salinity from CTD casts were used to calculate conservative temperature [°C] and absolute salinity (S_A [g kg^{-1}]), following the new thermodynamic equation of seawater (IOC et al., 2010).

In addition, satellite imagery was analyzed to give an overview of the dynamics in the Cape Basin. Sea Surface Temperature (SST) was derived from ODYSSEA, a Group for High Resolution Sea Surface Temperature (GHRSST) regional product

125 interpolated on a 0.02° grid for the South African area (Piollé and Autret, 2011; http://cersat.ifremer.fr/data/). The Sea Surface Height (SSH) and geostrophic velocity fields are derived from the Delayed Time Maps of Absolute Dynamic Topography (MADT) mapped daily on a 1/4° Mercator grid (Pujol et al., 2016). An eddy detection method based on the algorithm initially developed by Chaigneau et al. (2008) and modified by Laxenaire et al. (2017) was applied to these MADT fields. This method detected local MADT extrema to identify eddy centers with a lifetime of more than 7 days. After

130 identification of eddy centers, the spatially largest closed MADT contour line was defined as the boundary of the eddy. In

addition, each eddy was tracked at each time step within the boundary of the eddy defined at the previous time step, considering eddies splitting or merging.

3 Results

3.1 Dynamical background

135   The circulation around South Africa is dominated on the western part by the South Benguela upwelling frontal zone off the Cape Peninsula and on the eastern part by the Agulhas Current. These two features are visible in Figure 1, representing the 2015-annual averaged SST isotherms from the ODYSSEA dataset (color contours). The South Benguela upwelling zone inshore of the 500 m isobath extends all along the west coast and can generate a strong equatorward shelf-break front jet, the Cape Peninsula jet (Lutjeharms and Meeuwis, 1987; Nelson et al., 1998). The warm Agulhas Current, follows the shelf edge

140   southwestwards along the east coast. When it reaches 34°S, the current is affected by strong instabilities until it reflects at 38°S into the Indian Ocean (Lutjeharms and Cooper, 1996; de Ruijter et al., 1999; Lutjeharms, 2006). These instabilities are responsible for extensive meandering, and shear edge features such as Agulhas rings, eddies and filaments within this region. Agulhas ring observations, from shipboard surveys, were first exploited to quantify the energy, heat and salt fluxes of these features (*e.g.*, de Ruijter et al., 1999, and references therein). An independent estimate of the fluxes in the Cape Basin has

145   been accomplished by deploying a line of instruments across the pathway of Agulhas rings (BEST – Benguela Sources and Transports Experiment: Duncombe Rae et al. (1996); Garzoli and Gordon (1996); Goni et al. (1997)) and deep profiling floats (KAPEX – Cape of Good Hope Experiments: Lutjeharms et al. (1997); Richardson et al. (2003) and MARE – Mixing of Agulhas Rings Experiment - Van Aken et al. (2003)). Such measurements have demonstrated the highly turbulent regime of the Cape Basin (Boebel et al., 2003) and supplied important information on the propagation of Agulhas eddies. From these

150   experiments, the northwestward propagation of the rings in the Cape Basin was distinguished through a narrow ring corridor (Garzoli and Gordon, 1996) or through three different routes on the basis of topographic effects (Dencausse et al., 2010). During the measurement period of the tall-moorings along 34.5°S (September, 2014 to December, 2015), a total number of 16 Agulhas rings, defined as anticyclones that enter the Cape Basin crossing the C line (criteria of Laxenaire et al. (2017)), is estimated. From this altimetric tracking, the median radius and standard deviation of these features are equal to 85 ± 43 km

155   (66 ± 38 km considering the solid body rotation). The azimuthal speed of these Agulhas rings is equal to 0.49 ± 0.24 m s^{-1} with a translation speed, mainly northwestward of 7 ± 91 km day^{-1}. Considering our observing system along the eastern part of the SAMBA line, 11 anticyclonic and 7 cyclonic eddies influenced the mooring measurements at sites M1 (C1) to M4 (C4) (Fig. 2). Two of these anticyclonic eddies were generated at the Agulhas Retroflection and propagated into the Cape Basin through the northern route defined by Dencausse et al. (2010) (green line - Fig. 2). Six of the anticyclonic eddies

160   observed in this study are generated by the splitting of an Agulhas ring and three are generated north of the SAMBA line. All of the 7 cyclonic eddies are generated over the slope off the Cape Peninsula.

Ocean Science
Discussions

3.2 Upper ocean properties and dynamics

To characterize the hydrodynamical properties of these mesoscale features, the measurements of the upward-looking ADCP are analyzed concurrent with altimetry data.

165 From September 2014 to December 2015, the magnitude of the mean vertically averaged current (top 500-700 m of the water column) is between 12.1 ± 7.7 cm s^{-1} at the mooring nearest to the shelf (M1 - blue line, Fig. 3) and 25.5 ± 18.5 cm s^{-1} at the offshore mooring (M4 - red line, Fig. 3). Statistical comparisons between M1-M4 ADCP near-surface velocities and the surface geostrophic velocity derived from satellite altimetry have been made (Table II). Typically, the shallowest depth sampled (between 40 and 60 m depth) by the upward-looking ADCP was close to the surface but usually below the Ekman

170 layer. The comparison has been undertaken mostly in terms of correlation and root mean square differences between the zonal and meridional components of M1-M4 ADCPs (u_m, v_m) and those from altimetry at the nearest gridded location (u_{alti}, v_{alti}):

$$\Delta V_{rms} = \left[\frac{1}{N} \sum \left[\left(V_m - \overline{V_m} \right) - \left(V_{alti} - \overline{V_{alti}} \right) \right]^2 \right]^{1/2} \quad (1)$$

with V the zonal or the meridional components of the velocity and m the index of the mooring. Additionally, comparisons

175 were made by computing the bias (Eq. 2).

$$bias = \overline{V_m} - \overline{V_{alti}} \quad (2)$$

Values of the correlation coefficient between ADCP and altimetry velocity estimates (R) fell in the range 0.30-0.83, and ΔV_{rms} varied from 12.9 to 15.9 cm s^{-1} (Table II). The absolute values of the biases were typically between 1 and 5 cm s^{-1}, with a maximum of 8.8 cm s^{-1} at M2. Correlation between the u-component of these velocity measurements showed values greater

180 than 0.7 for the three offshore moorings. Weak correlation coefficients for both components were observed for the mooring closest to the shore (M1, 1121 m of depth). The coefficient for the v-component gradually increases across the continental slope, moving away from the shelf. The correlations for sites away from the shelf are significant considering the mean zonal correlation scales of the satellite product of 150 km at that latitude [Pujol et al., 2016]. The poor correlation for both velocity components at M1 can be mainly attributed to its position too close to the coast (~160 km off shore, at the shelf break), and

185 therefore embedded in a different dynamical context than purely geostrophic, and a possible geostrophic shear between the surface and the first level of measurement. The comparisons reveal that satellite data provides an accurate description of the upper ocean circulation across the continental slope along our mooring arrays, except near the shelf-break (*i.e.*, well inshore of the 1200 m isobath).

In light of these results, we are confident that the variability of the zonal and meridional components of the upper-layer

190 velocity from the offshore moorings (M2 to M4) can be analyzed according to the dynamics inferred from satellite altimetry. The currents measured during September 2014 - December 2015 in the top 500 m of the water column contain a number of sudden rotational events, seen in the time series of the two velocity components (Figure 3). These transitions in the velocity field tend to be associated with mesoscale eddies passing through the mooring line. The altimetry data allows us to examine

the impact of 7 cyclonic (blue shaded areas - Fig. 3) and 11 anticyclonic eddies (red shaded areas - Fig. 3) on zonal and

195 meridional velocity at the four mooring sites. Moreover, the data records show that the presence of dipoles affects the velocity measurements (we have observed 4 of such events: yellow shaded areas - Fig. 3). All these mesoscale features have a closed contour in the satellite dynamic-height amplitude of at least 10 cm.

To have more of a consistent and complete picture of the dynamics associated within the Cape Basin, the position of these eddies observed by satellite altimetry were analyzed in relation to variations in the ODYSSEA SST field (Figure 4). On

200 September 19, 2014 the eddy identification method detects one cyclonic eddy (C1) and one anticyclonic eddy (A2) close enough to the mooring line to affect the measurement (Fig. 4a). This dipole influences the upper-ocean water velocity at M4 with a depth-averaged maximum of 33.4 cm s^{-1} (Tab. III). Approximately one month later (Fig. 4b), C1 is still positioned over M4 and A2 has propagated southeastward. The dipole created by the interaction of these two eddies induces a westward current associated with a warm and relatively wide filament detected at all the moorings (M1-M4). On December 1, 2014

205 (Fig. 4c), C1 moves westward still affecting the currents at M4. The generation of anticyclone A8 gives rise to a second dipole with C1, which, again, generates the propagation of a warm filament between these features. On December 19 (Fig. 4d), A8 had merged with A4, an Agulhas ring (characterized by a mean radius of 170 km) south of the SAMBA line. At that time, a new cyclonic eddy (C7) was generated on the slope, at the South Benguela upwelling front, south of the mooring line. After two months (Fig. 4e), a transient anticyclonic eddy (A12) is present between M3 and M4 and a new cyclonic eddy

210 (C9) is generated at 35°S. This cyclonic eddy affects the measurements of M2-M3 until the end of March, increasing the zonal velocity over the slope up to 104.3 cm s^{-1} at M3 (Fig. 3d, Tab. III). This strong northeastward current is also intensified by an intense cross-shelf density front that is enhanced at that time due to an upwelling event (Fig. 4f) and the northward migration of an Agulhas ring A13 (Fig. 4g). On March 21, 2015, A13 splits to generate A16. This anticyclonic eddy was close enough to M4 to induce the northward propagation of a warm filament on April 3, 2015 (Fig. 4h). At the end of April, a

215 new dipole due to the interaction of eddies A19 and C14 is generated around M4. This intense dipole induced a strong northward current that injected cold surface water across the mooring array in April (Fig. 4i) and warmer Agulhas Current water during the month of May (Fig. 4j,k). This injection of warm water is boosted by the presence of another dipole present around 38°S (C16-A17). After this intense event, the satellite imagery reveals the presence of a cyclonic eddy (C17) in June, generated by the splitting of C14 (Fig. 4k,l) and an anticylonic eddy (A24) in July (Fig. 4m) between M3 and M4. On

220 September 15, 2015 (Fig. 4n), a new dipole (A26, C23) generates a warm filament propagating toward M4. Finally, at the end of this time series, an anticyclonic eddy (A34) associated with 2 small cyclonic eddies (C23, C25) are observed over the SAMBA line.

To synthesize, the moorings over the slope (M1, M2 and M3) are affected by seven cyclonic eddies and two anticyclonic eddies (Table III). M3 undergoes to the influence of two more anticyclonic eddies crossing the SAMBA line more off-shore.

225 These also impact M4. The largest velocities perturbation at the upper-slope moorings are associated to cyclonic eddy C9. M4 records show the influence of all the anticyclonic eddies and four cyclonic eddies. Largest velocity perturbations are seen at M4 during the presence of the dipole A19 and C14.

3.3 Case studies - Upper water column

From the combined analysis of satellite and mooring data in section 3.2, four case studies have been selected to reveal the
230   vertical–temporal structure of eddy-like features and filaments (Figures 5 and 6), and strong intrusions of cold water or
Agulhas Current water due to eddy-eddy interactions (Figures 7 and 8). We focus on the variability at M4 which exhibits the
strongest variations in responses to passing mesoscale features.

Case Anticyclonic Eddy: From the middle to the end of March (Fig. 5a), M4 is impacted by Agulhas ring A13. The velocity
magnitude maxima during this period reaches 60.4 cm s^{-1}. The vertical-temporal section of the u-component of the current
235   speed (Fig. 5c) shows an eddy-like structure from March 14 to March 24, 2015. The core of this westward current defined by
the velocity magnitudes greater than 50 cm s^{-1}, penetrates down to 230 m, is associated with the circulation around the
northern side of A13. During this period, an increase of temperature (salinity) of 2.4°C (0.3470) is recorded at the SBE37
MicroCat's at 450 m depth (Fig. 5e). This large Agulhas ring splits on March 21 to generate A16 and induces a second
maxima in the velocity magnitude at M4 reaching 42.2 cm s^{-1}. This northward current from the surface to 175 m depth (Fig.
240   5c) is associated with the propagation of a warm filament at the eastern side of A16 (Fig. 5b). From the satellite altimetry
(colored circles at the top of Fig. 5c,d), the velocity component magnitudes are lower than the ones from the upward-looking
ADCP but show similar order values.

Case Cyclonic Eddy: The same analysis is done for a second event occurring late September. On September 15, 2015 (Fig.
6a), a dipole (A26, C23) affects the circulation along the SAMBA line. The dipole advects a warm filament propagating
245   westward across M4 (Fig. 6c). The maxima of the velocity magnitude increases until 52.4 cm s^{-1} on September 18. This
feature generates northward flow across M4 with core speeds of 40 cm s^{-1} which extend from the surface to 250 m. C23
originally generates one month earlier on the slope off the Cape Peninsula, north of the SAMBA line, is closest to M4 on
September 26 (Fig. 6b) affecting the measurements at this mooring. The vertical time sections of the components of the
speed (Fig. 6c,d) show a northwestward current from September 19 to October 8 associated with the circulation at the
250   southeastern side of C23. This northwestward current is also caught by the altimetry data particularly for the u-component
(Fig. 6c – colored dots). This strong cyclonic eddy (68.7 cm s^{-1} maximal velocity magnitude), has core speeds of 40 cm s^{-1}
that extend from the surface down past 400 m generates a decrease of salinity and temperature at 500 m depth of 0.33 and
3.5°C respectively. From the satellite altimetry (colored circles at the top of Fig. 6c,d), the zonal component of the current
speed is in good agreement with the upward-looking ADCP compared to the meridional one which shows lower velocity.

255   Case Cold and Warm Intrusion: From the end of April to the middle of May (Figures 7 and 8), anticyclonic eddy A19 and
cyclonic eddy C14 affect the circulation around M4. This intense dipole induces an intense northward current with a
maximal velocity magnitude of 115.7 cm s^{-1} on April 22 (Fig. 7a,d) and 104.5 cm s^{-1} on May 13 (Fig. 8a,d). These two events
last about 22 and 15 days respectively. Their vertical influence is deeper than 600 m depth. The vertical mooring motion as
evidenced by the downward shifts in the range of depths resolved by the ADCPs is very intense during these two events.
260   According to the different pressure sensors, the performance of the mooring's design is fully satisfactory. The altimetry data

show the same intense northward current at the surface, however there is a pronounced lag of 7 days for the second intrusion. This lag is no longer present if we consider the altimetric velocity one grid eastward (0.25° of resolution). The first northward intrusion injects in the upper part of the water column, initially cooler (ΔT=-6.2°C) and fresher (ΔS=-0.73) water of possibly Subantarctic origins (Fig. 7e) and the second intrusion injects a warmer (ΔT=+3.9°C) and saltier (ΔS=+0.42) water of Indian origins (Fig. 8e).

3.4 Full water column water masses distribution and variability

We used the daily-averaged temperature and salinity data obtained from SBE37 MicroCat's instruments on moorings to recover the time series of the regional water masses for each mooring. Figure 10 show the resulting time series. The color codes we used refer to the specific regional water masses. Similar to Lamont et al. (2015), the vertical distribution of water masses was determined according to Conservative Temperature, Absolute salinity, and density layers, as illustrated in Figure 9. Modified Upwelled Water (MUW) was defined according to Duncombe Rae (2005), while the criteria of Donners et al. (2005) were used to define Oceanic Surface Water (OSW), light South Atlantic Central Water (lSACW - defined as Indian Central Water brought into the South Atlantic Ocean by Agulhas Current intrusions), South Atlantic Subtropical Mode Water (SASTMW), and Subantarctic Mode Water (SAMW- with a vertical temperature gradient less than 1.6 °C/100 m (Roemmich and Cornuelle, 1992)). A new water mass, called Agulhas Ring Mode Water (ARMW) has been identified recently by Capuano et al. (2017). ARMW is defined as a local ventilation of Indian Central waters and is identified inside different sampled Agulhas rings (Ducombe Rae et al., 1996; Arhan et al 1999; McDonagh et al., 1999, Gladyshev et al., 2008, Arhan et al., 2011). Three different varieties of Antarctic Intermediate Water (AAIW), namely Indian AAIW (I-AAIW) with $S_A \geq$ 34.47 g kg^{-1}, Indo-Atlantic AAIW (IA-AAIW) with $34.37 \leq S_A \leq 34.47$ g kg^{-1}, and Atlantic AAIW (A-AAIW) with $S_A \leq$ 34.37 g kg^{-1}, were characterized according to Rusciano et al. (2012). Upper Circumpolar Deep Water (UCDW) was defined as $27.55 < \gamma^n < 27.92$ kg m^{-3}, North Atlantic Deep Water (NADW) as $27.92 < \gamma^n < 28.11$ kg m^{-3}, and Lower Circumpolar Deep Water (LCDW) as $28.11 < \gamma^n < 28.26$ kg m^{-3} (Heywood and King, 2002).

Overall, the vertical distribution of water masses at M3 and M4 shows that SAMW stabilizes on the southwestern African continental slope around 500 m depth, I-AAIW between 500 and 1000 m, UCDW from 1000 to 1500 m depth, NADW between 1600 and 3000 m, and finally LCDW below 3000 m (Fig. 10). This mean vertical and zonal distributions are affected by the regional mesoscale dynamic described in the previous section. Typically a cyclonic (anticyclonic) eddy causes uplift (suppression) of isopycnal layers and therefore of water masses. Moreover, it is particular evident that when anticyclonic eddies cross the moorings, usually AAIW variety changes from I-AAIW to IA-AAIW, while UCDW is found deeper than 1500 m (*e.g.*, on March in 2015, at M4). During the cyclonic eddies, a general uplift of I-AAIW, UCDW and LCDW is observed (*e.g.*, on October in 2014, at M4). The full-depth time series shows that these events influence the upper part of the water column but they also affect most of the water column, down to 3000 m of depth. During the two successive intrusions of cold and warm waters due to the presence of dipoles on April-May in 2015, at M4, the different pressure

sensors show similar strong vertical variation confirming the performance of the mooring's design. During this time period, the water masses are affected by successive downwelling/upwelling events. Interestingly, no A-AAIW is observed in the

295 mooring records during the whole 450-day deployment.

3.5 Full-water-column analysis – Focus on the 4 case studies

The different data sets allow us to analyze in more details the effects of the mesoscale features described in the previous sections and successful cross-validate the measurements made by the different types of moored instruments (tall-moorings *vs.* CPIES).

300 The daily sub-sampled data from the CPIES includes ocean currents 50 m above the seafloor, bottom pressure, and τ, the round trip acoustic travel time. An empirical lookup table for hydrographic property profiles is used in conjunction with measured τ to obtain full-water-column profiles of temperature and salinity. This technique known as the "Gravest Empirical Mode" (GEM) method (Meinen and Watts, 2000; Watts et al., 2001) was constructed from 115 CTD and Argo profiles in the region. The GEM method has been successfully applied in the eastern South Atlantic (Meinen et al., 2013). Combining τ

305 measurements from C4 (Tab. I) with the GEM look-up tables produces daily full-water-column hydrographic profiles at this position. The profiles estimated via the GEM method can be compared with the single points values of temperature and salinity from M4 sensors (8 sensors recording over the common time period, from September 20, 2014 to August 11, 2015). The reconstructed field captures the major changes of the temperature and salinity variability in the upper water column. Indeed, significant correlation coefficients between these two data sets show values higher than 0.95 for salinity and

310 temperature at the shallowest sensors (~450, 900 m depth). At the deepest levels, the correlation coefficients range between -0.10 and 0.79 are not significant at the 95% confidence level. To determine the significance of the correlations, the number of independent sample or degrees of freedom is estimated by dividing the record length by twice the integral time scale of the variability of the respective quantity (~40 days; Thomson and Emery, 2014).

Measurements from these two data sets are compared for the four case studies described in Section 3.3: Cyclonic eddy,

315 Anticyclonic eddy, Cold intrusion, and Warm intrusion. The temperature and salinity percent changes at M4 due to the presence of the eddy structures (C23 and A13, Fig. 11a,b) and the intrusions of cold and warm water (Fig. 11c,d) are calculated relative to the hydrographic properties in "normal conditions" (just before each event occurred).

During the occupancy of A13 at M4 (March 17 to April 1, 2015), the measurements at the SBE37 MicroCat's show an increase of temperature in the upper water column at 450 and 900 m (percent changes of 9% and 8% respectively; Fig. 11a -

320 red dots). An increase is also recorded for the salinity at the shallowest sensor (percent changes of 0.38%; Fig. 11b - red dot). The reconstructed temperature profile via the GEM method in the upper 1000 m depth captures a maxima of temperature anomaly at 760m (Fig. 11a - red line) which is not measured with the single point measurement of the tall-mooring but matches well the values at the depth of the MicroCat's. Concerning the salinity (Fig. 11b - red line), the maximum is shallower near 450 m and is well resolved by the vertical sampling of the SBE37 MicroCat's. From these measured and

325 reconstructed properties, we have evaluated the water masses associated with this Agulhas ring (Fig. 9 – yellow square, SBE

and circles, CPIES). The upper and intermediate layers are characterized by MUW at the surface, SASTMW at 438 db, and SAMW at 770 db. For the deep-water column, as said before the reconstructed fields from CPIES are not significantly correlated (dashed line Fig. 11) compared with SBE37 MicroCat's data. Nevertheless, the reconstructed fields and the SBE37 MicroCat's sensors deeper than 1500 m highlight a warming until 4400 m depth. This deep warming confirm the downlift of

330 isopycnal layers and therefore of UCDW and NADW.

During the time period of C23 (September 14-28, 2015), there is hydrographic data from the SBE37 MicroCat's. However, hydrographic profile can not be estimated from the CPIES as the event happened after its recovery and re-deployment. The SBE37 MicroCat's at 450 m depth records colder and fresher water. Decreases of 13% for the temperature and of 0.35% for the salinity (Fig. 11a,b - blue dots) highlight an uplift of I-AAIW at this depth, confirmed by the water masses definition

335 (Fig. 9 – greed square). Moreover, at the second sensor (900 m depth), a positive gain coefficient for the salinity is recorded confirming the upwelling of UCDW. Negligible anomalies are detected in the deeper part of the water column.

During the intrusions of Subantarctic water (April 22, 2015- May 5, 2015) and warm Indian water (May 11-23, 2015), the sensor's recording depths are deeper than the previous case studies due to strong mooring vertical motion (Fig. 11c,d). The temperature and salinity percent changes for the warm intrusion is clearly observed by the SBE37 MicroCat's at 550 m depth

340 (Fig. 11c,d - red dots and lines). Regarding the cold intrusion (Fig. 11c,d - blue dots and lines), the temperature (salinity) maximum anomaly of the reconstructed salinity is deeper (shallower) that the first measurement of the tall-mooring. For both intrusions, the gain coefficients come out much larger than for the eddies (for example, during the cold intrusion gain coefficients reach -24% for the temperature and -0.8% for the salinity). The reconstructed gain coefficients agree well with the values determined from the SBE37 MicroCats during both the warm and cold intrusion events. From the reconstructed

345 CPIES fields, the surface temperature and salinity signatures of both intrusions show value in the range of OSW (Fig. 9- pink (warm) and blue (cold) circles). At intermediate depths (between 450 to 720 db), the characteristics of I-AAIW and SAMW are detected. Interestingly from the SBE37 MicroCat's and the reconstructed fields, we observe strong variations of temperature between 3500 and 4200 m for both events. The presence of such warm and cold water anomalies at these depths reveal the impact of the upper-ocean mesoscale structures on the whole water column.

350 **4 Discussion and concluding remarks**

Since 2010, several efforts have resulted to enhance further AMOC observing systems in the South Atlantic. This strategic monitoring system continues to grow along 34.5°S, a crucial latitude to evaluate the AMOC variability and the impact of inter-ocean exchanges. As a consequence of the limitations of high spatial and temporal scales *in situ* observations, the quantification of inter-ocean exchange is still an ongoing work and many key questions and issues remain open such as

355 which are the characteristics and the impact of mesoscale structures on local water masses distribution. In the framework of the SAMOC project, we provide here further investigation using a combination of satellite altimetry, tall-moorings measurements and CPIES records.

Focusing on the eastern part of the SAMBA array, the general circulation around South Africa has been rather well described in previous studies. Two main processes have been observed to influence this area: an equatorward shelf-break front jet off
360 the Cape Peninsula (Lutjeharms and Meeuwis, 1987; Nelson et al., 1998) and the instabilities of the Agulhas Current responsible for the spawning of mesoscale eddies propagating into the Cape Basin (Lutjeharms and Cooper, 1996; de Ruijter et al., 1999; Lutjeharms, 2006).

During the time period of our study (~14 months), we objectively identified from satellite altimetry 16 anticyclonic eddies as Agulhas rings. The eddy statistics (diameter of 170 ± 86 km with translation speeds of 7 ± 91 km day^{-1}) are in good
365 agreement with previous estimates. The comparisons reveal that satellite data provides an accurate description of the upper ocean circulation across the continental slope along our mooring arrays, except near the shelf-break (i.e., along and inshore of the 1200 m isobath). The joint analysis of both, satellite and mooring data, shows that the eastern mooring array is strongly affected by the regional intense mesoscale dynamics generated by instabilities of the South Benguela upwelling front and the presence of Agulhas Rings. These processes induce intense intra-seasonal upper-ocean velocity variations and
370 water masses exchanges across both, the shelf and the open ocean and between subantarctic and subtropical frontal zones.

The upper-slope moorings (M1 and M2) show to be affected essentially by cyclonic eddies generated at the South Benguela upwelling front, while the deeper slope moorings (M3 and M4) are affected by the more complex dynamics characterizing the Cape Basin and involving both, Agulhas Rings and cyclonic eddies. Previous studies (Arhan et al., 1999, 2011; Schouten et al., 2000; Boebel et al., 2003) have shown that Agulhas rings coexist with cold-core (cyclonic) eddies, which have a
375 smaller diameter (120 km) and drift across the northwestward migration path of the anticyclones. These cyclonic eddies can contribute directly to the input of Indian water in the Atlantic (Lutjeharms et al., 2003; Arhan et al., 2011) or indirectly via the formation of filaments (Lutjeharms and Cooper, 1996; Whittle et al., 2008). Interaction of cyclonic and anticyclonic eddies can be responsible for the extraction of warm Agulhas water plumes. These filaments may provide not more than 15% of the total mass flux (Lutjeharms and Cooper, 1996).

380 The presence of cyclonic eddies, filaments and interaction of cyclonic and anticyclonic eddies have been also described in more details in this study with our four case studies. The different properties of each event have been compared between tall-moorings and CPIES measurements allowing a better characterization of the full-water column hydrographic properties. The reconstructed fields capture the major changes of the temperature and salinity variability in the upper water column. In particular, they show the typical impact of cyclonic and anticyclonic eddies causing, respectively, an uplift and downward
385 motion of isopycnal layers and therefore of water masses. It has been shown that the trapping depth of rings can reach the sea floor (Van Aken et al., 2003). This influence can extend till the deepest layers. Indeed, as already suggested by Van Aken et al. (2003) for Agulhas rings, the analyses of our tall mooring deep SBE MicroCat data show that not only Agulhas ring but also cyclonic eddy and cold/warm water intrusions can reach 4400 m of depth impacting the UCDW and NADW layers.

Our study indicates that exchanges of water masses across the continental slope happen through water advection via not
390 only mesoscale eddies but also wide filaments engendered by the interaction between eddies, and in particular, through the existence of intense dipoles. As illustrated in previous studies, such filaments can extend well in to the thermocline and can

12

be related to dipole dynamics (de Steur et al., 2004; Baker-Yeboah et al., 2010). Such wide intrusions are defined as intense north- northwestward current affecting directly the upper 1500 m and indirectly through the whole water column. These injections are different from filaments, which exhibit a much smaller vertical extension (around 300 m of the water column).

395 Among the different processes observed along the eastern SAMBA array, the most significant event is the intrusion of waters of Indian and subantarctic origin. In terms of number of occurrence of each event during the 14 months of record, we account for one intrusion of cold and warm waters, eight Agulhas rings and four warm filaments. Our work suggest that not only the advection of water within Agulhas rings or cyclonic eddies is important but that also intrusions and filaments have a significant impact on the total mass, heat, and salt fluxes and therefore, they all need to be better accounted.

400 Moreover, this study presents the first comparison between data sets and supports the validation of the reconstructed field with the GEM technique in the upper water column. Here properties are fully resolved by the local sensors and by the GEM reconstructed fields. At intermediate depths (between 400 and 700 db), the presence of SAMW and SASTMW are identified within Agulhas rings and intrusions of warm and cold waters. ARMW characteristics are not clearly evidence in our case studies. This fact can be attributed to the distance of the structures from the moorings, the low vertical resolution sampling in

405 the upper 500 m, and the mixing associated with the mesoscale activity in the Cape Basin which can result in substantial uplift and downwelling of waters. The deep-water column properties remain to be analyzed with local temperature and salinity sensors. Moreover, the distance between CPIES and tall-moorings (*e.g.* 210 km between M3 and M4) complicates transport estimates -as the decorrelation length scale is smaller than this distance.

Finally, this strategic monitoring system continues to grow with international collaborative projects on the specific goal of

410 quantify the AMOC variability along 34.5°S. These first independent observations comparison in the eastern part of the SAMBA array gives some confidence in these preliminary results. Future investigations with longer time series at these existing sites will lead to a better understanding of the eastern boundary current variability and Indo-Atlantic exchanges, and ultimately improve our understanding of the strength and variability of the AMOC.

Ocean Science

Discussions

Open Access

EGU

References

430

Ansorge, I. J., Speich, S., Lutjeharms, J. R. E., Goni, G. J., Rautenbach, C. D. W., Froneman, P. W., Rouault, M. and Garzoli, S. (2005). Monitoring the oceanic flow between Africa and Antarctica: report of the first GoodHope cruise: research in action. S. Afr. J. Sci., 101(1-2), 29-35.

Ansorge, I. J., Baringer, M. O., Campos, E. J. D., Dong, S., Fine, R. A., Garzoli, S. L., Goni, G., Meinen, C. S., Perez, R. C.,
435 Piola, A. R., Roberts, M. J., Speich, S., Sprintall, J., Terre, T. and Van den Berg, M. A. (2014). Basin-Wide Oceanographic Array Bridges the South Atlantic. Eos, Transactions American Geophysical Union, 95(6), 53-54, doi:10.1002/2014EO060001.

Arhan, M., Mercier, H. and Lutjeharms, J. R. E. (1999). The disparate evolution of three Agulhas rings. J. Geophys. Res., 104(C9), 20987-21005, doi:10.1029/1998JC900047.

440 Arhan, M., Speich, S., Messager, C., Dencausse, G., Fine, R. and Boye, M. (2011). Anticyclonic and cyclonic eddies of subtropical origin in the subantarctic zone south of Africa. J. Geophys. Res., *116*(C11), doi:10.1029/2011JC007140.

Baker-Yeboah, S., Flierl, G. R., Sutyrin, G. G. and Zhang, Y. (2010). Transformation of an Agulhas eddy near the continental slope, Ocean Sci., 6, 143-159, doi:10.5194/os-6-143-2010.

van Ballegooyen, R. C., Gründlingh, M. L. and Lutjeharms, J. R. (1994). Eddy fluxes of heat and salt from the southwest
445 Indian Ocean into the southeast Atlantic Ocean: A case study. J. Geophys. Res., 99(C7), 14053-14070, doi: 10.1029/94JC00383.

Baringer, M. O. N. and Larsen, J. C. (2001). Sixteen years of Florida Current transport at 27°N. Geophys. Res. Lett., 28(16), 3179-3182, doi: 10.1029/2001GL013246.

van den Berg, M. A. (2015). Cruise report: SAMBA - Moorings and Monitoring Line, RS Algoa Voyage 221, 30 November -
450 6 December 2015. Department of Environmental Affairs Cruise Reports.

Beal, L. M., De Ruijter, W. P., Biastoch, A. and Zahn, R. (2011). On the role of the Agulhas system in ocean circulation and climate. Nature, 472(7344), 429-436, doi:10.1038/nature09983.

Biastoch, A., Böning, C. W. and Lutjeharms, J. R. E. (2008). Agulhas Leakage dynamics affects decadal variability in Atlantic overturning circulation. Nature, 456, 489–492, doi: 10.1038/nature07426.

455 Bingham, R. J., Hughes, C. W., Roussenov, V. and Williams, R. G. (2007). Meridional coherence of the North Atlantic meridional overturning circulation. Geophys. Res. Lett., 34, L23606, doi: 10.1029/2007GL031731.

Boebel, O., Lutjeharms, J., Schmid, C., Zenk, W., Rossby, T. and Barron, C. (2003). The Cape Cauldron: a regime of turbulent inter-ocean exchange. Deep Sea Res., Part II, 50(1), 57-86, doi: 10.1016/S0967-0645(02)00379-X.

Broecker, W. S. (1991). The great ocean conveyor. Oceanography, 4(2), 79-89. Retrieved from
460 http://www.jstor.org/stable/43924572.

Byrne, D. A., Gordon, A. L. and Haxby, W. F. (1995). Agulhas eddies: A synoptic view using Geosat ERM data. J. Phys. Oceanogr., 25(5), 902-917, doi: 10.1175/1520-0485(1995)025<0902:AEASVU>2.0.CO;2.

Capuano, T., Speich, S. and Carton, X. (submitted, 2017). Mesoscale and submesoscale processes in the southeast Atlantic and their impact on the regional thermohaline structure. J. Geophys. Res.

465 Chaigneau, A., Gizolme, A. and Grados, C. (2008). Mesoscale eddies off Peru in altimeter records: Identification algorithms and eddy spatio-temporal patterns. Prog. Oceanogr., 79(2), 106-119, doi: 10.1016/j.pocean.2008.10.013.

Chereskin, T. K., Donohue, K. A., Watts, D. R., Tracey, K. L., Firing, Y. L. and Cutting, A. L. (2009). Strong bottom currents and cyclogenesis in Drake Passage. Geophys. Res. Lett., 36(23), doi: 10.1029/2009GL040940.

Cunningham, S. A., Kanzow, T., Rayner, D., Baringer, M. O., Johns, W. E., Marotzke, J., Longworth, H. R., Grant, E. M.,
470 Hirschi, J. J.-M., Beal, L. M., Meinen, C. S. and Bryden, H. L. (2007). Temporal variability of the Atlantic meridional overturning circulation at 26.5°N. Science, 317(5840), 935-938, doi: 10.1126/science.1141304.

De Steur, L., Van Leeuwen, P. J., & Drijfhout, S. S. (2004). Tracer leakage from modeled Agulhas rings. J. Phys. Oceano., 34(6), 1387-1399, doi:10.1175/1520-0485(2004)034<1387:TLFMAR>2.0.CO;2.

Dencausse, G., Arhan, M. and Speich, S. (2010). Routes of Agulhas rings in the southeastern Cape Basin. Deep Sea Res.,
475 Part I, 57(11), 1406-1421, doi: 10.1016/j.dsr.2010.07.008.

Donners, J., Drijfhout, S. S. and Hazeleger, W. (2005). Water mass transformation and subduction in the South Atlantic. J. Phys. Oceano., 35(10), 1841-1860, doi: 10.1175/JPO2782.1.

Duncombe Rae, C. M. (1991). Agulhas retroflection rings in the South Atlantic Ocean: an overview. Afr. J. Marine Sci., 11(1), 327-344, doi: 10.2989/025776191784287574.

480 Duncombe Rae, C. M., Garzoli, S. L. and Gordon, A. L. (1996). The eddy field of the southeast Atlantic Ocean: A statistical census from the Benguela Sources and Transports Project. J. Geophys. Res., 101(C5), 11949-11964, doi: 10.1029/95JC03360.

Duncombe Rae, C. M. (2005). A demonstration of the hydrographic partition of the Benguela upwelling ecosystem at 26°40'S. Afr. J. Mar. Sci., 27(3), 617-628, doi: 10.2989/18142320509504122.

485 Elipot, S., Frajka-Williams, E., Hughes, C. W., Olhede, S. and Lankhorst, M. (2017). Observed basin-scale response of the North Atlantic meridional overturning circulation to wind stress forcing. J. Climate, 30(6), 2029-2054, doi: 10.1175/JCLI-D-16-0664.1.

Garzoli, S. L. and Gordon, A. L. (1996). Origins and variability of the Benguela Current. J. Geophys. Res., 101(C1), 897-906, doi: 10.1029/95JC03221.

490 Garzoli, S. L., and Matano, R. (2011). The South Atlantic and the Atlantic meridional overturning circulation. Deep Sea Res., Part II, 58(17), 1837-1847, doi: 10.1016/j.dsr2.2010.10.063.

Gladyshev, S., Arhan, M., Sokov, A. and Speich, S. (2008). A hydrographic section from South Africa to the southern limit of the Antarctic Circumpolar Current at the Greenwich meridian. Deep Sea Res., Part I, 55(10), 1284-1303, doi: 10.1016/j.dsr.2008.05.009.

495 Goni, G. J., Garzoli, S. L., Roubicek, A. J., Olson, D. B. and Brown, O. B. (1997). Agulhas ring dynamics from TOPEX/POSEIDON satellite altimeter data. J. Mar. Res., 55(5), 861-883, doi: 10.1357/0022240973224175.

Gordon, A. L. (1986). Interocean exchange of thermocline water. J. Geophys. Res., 91, 5037–5046, doi: 10.1029/JC091iC04p05037.

Gordon, A. L. and Haxby, W. F. (1990). Agulhas eddies invade the South Atlantic: Evidence from Geosat altimeter and
500 shipboard conductivity-temperature-depth survey. J. Geophys. Res., 95(C3), 3117-3125, doi: 10.1029/JC095iC03p03117.

Gordon, A. L., Weiss, R. F., Smethie, W. M. and Warner, M. J. (1992). Thermocline and intermediate water communication between the South Atlantic and Indian Oceans. J. Geophys. Res., 97(C5), 7223-7240, doi: 10.1029/92JC00485.

Gladyshev, S., Arhan, M., Sokov, A. and Speich, S. (2008). A hydrographic section from South Africa to the southern limit of the Antarctic Circumpolar Current at the Greenwich meridian. Deep Sea Res., Part I, 55(10), 1284-1303, doi:
505 10.1016/j.dsr.2008.05.009.

Heywood, K. J. and King, B. A. (2002). Water masses and baroclinic transports in the South Atlantic and Southern oceans. J. Mar. Res., 60(5), 639-676, doi: 10.1357/002224002762688687.

Hummels, R., Brandt, P., Dengler, M., Fischer, J., Araujo, M., Veleda, D. and Durgadoo, J. V. (2015). Interannual to decadal changes in the western boundary circulation in the Atlantic at 11°S. Geophys. Res. Lett., 42(18), 7615-7622, doi:
510 10.1002/2015GL065254.

IOC, Scor, IAPSO, 2010. The International Thermodynamic Equation of Seawater 2010: Calculation and Use of Thermodynamic Properties. Intergovernmental Oceanographic Commission, Manuals and Guides No. 56.

Kanzow, T., Cunningham, S. A., Rayner, D., Hirschi, J. J.-M., Johns, W. E., Baringer, M. O., Bryden, H. L., Beal, L. M., Meinen, C. S. and Marotzke, J. (2007). Observed flow compensation associated with the MOC at 26.5°N in the Atlantic.
515 Science, 317(5840), 938-941, doi: 10.1126/science.1141293.

Lamont, T., Hutchings, L., Van Den Berg, M. A., Goschen, W. S. and Barlow, R. G. (2015). Hydrographic variability in the St. Helena Bay region of the southern Benguela ecosystem. J. Geophys. Res., 120(4), 2920-2944, doi: 10.1002/2014JC010619.

Laxenaire, R., Speich, S., Blanke, B., Chaigneau, A. and Pegliasco, C. (resubmitted after revision, 2017). Agulhas Ring
520 trajectories connecting western boundaries as inferred from altimetry. Geophys. Res. Lett.

Lozier, M. S. (2010). Deconstructing the conveyor belt. Science, 328(5985), 1507-1511, doi: 10.1126/science.1189250.

Lutjeharms, J. R. E. and Meeuwis, J. M. (1987). The extent and variability of South-East Atlantic upwelling. Afr. J. Marine Sci., 5(1), 51-62, doi: 10.2989/025776187784522621.

Lutjeharms, J. R. E. and Cooper, J. (1996). Interbasin leakage through Agulhas Current filaments. Deep Sea Res., Part I,
525 43(2), 213217-215238, doi: 10.1016/0967-0637(96)00002-7.

Lutjeharms, J. R. E., Boebel, O. and Rossby, T. (1997). KAPEX: an international experiment to study deep water movement around southern Africa. S. Afr. J. Sci., 93, 377-381.

Ocean Science
Discussions

Lutjeharms, J. R. E., Boebel, O. and Rossby, H. T. (2003). Agulhas cyclones. Deep Sea Res., Part II, 50(1), 13-34, doi: 10.1016/S0967-0645(02)00378-8.

530   Lutjeharms, J. R. E. (2006). The Agulhas Current. Springer Berlin Heidelberg, 329pp, doi:10.1007/3-540-37212-1.

McCarthy, G. D., Smeed, D. A., Johns, W. E., Frajka-Williams, E., Moat, B. I., Rayner, D., Baringer, M. O., Meinen, C. S., Collins J. and Bryden, H. L. (2015). Measuring the Atlantic meridional overturning circulation at 26°N. Prog. Oceanogr., 130, 91-111, doi: 10.1016/j.pocean.2014.10.006.

McCartney, M. S. (1977). Subantarctic Mode Water, A Voyage of Discovery, edited by M. Angel , 103-119pp, Pergamon,
535   New York.

McDonagh, E. L., Heywood, K. J. and Meredith, M. P. (1999). On the structure, paths, and fluxes associated with Agulhas rings. *J. Geophys. Res.*, *104*(C9), 21007-21020, doi:10.1029/1998JC900131.

Meinen, C. S and Watts, D. R. (2000). Vertical structure and transport on a transect across the North Atlantic Current near 42°N: Time series and mean. J. Geophys. Res., 105(C9), 21869-21891, doi: 10.1029/2000JC900097.

540   Meinen, C. S., Piola, A. R., Perez, R. C. and Garzoli, S. L. (2012). Deep Western Boundary Current transport variability in the South Atlantic: preliminary results from a pilot array at 34.5° S. Ocean Sci., 8(6), 1041-1054, doi: 10.5194/os-8-1041-2012.

Meinen, C. S., Speich, S., Perez, R. C., Dong, S., Piola, A. R., Garzoli, S. L., Baringer, M. O., Gladyshev, S. and Campos, E. J. D. (2013), Temporal variability of the meridional overturning circulation at 34.5ºS: Results from two pilot boundary arrays
545   in the South Atlantic. J. Geophys. Res., 118, 6461–6478, doi:10.1002/2013JC009228.

Meinen, C. S. and Garzoli, S. L. (2014). Attribution of Deep Western Boundary Current variability at 26.5°N. Deep Sea Res., Part I, 90, 81-90, doi: 10.1016/j.dsr.2014.04.016.

Meinen, C. S., Garzoli, S. L., Perez, R. C., Campos, E., Piola, A. R., Chidichimo, M. P., Dong, S. and Sato, O. T. (2017). Characteristics and causes of Deep Western Boundary Current transport variability at 34.5°S during 2009-2014. Ocean Sci.,
550   13(1), 175, doi: 10.5194/os-13-175-2017.

Nelson, G., Boyd, A. J., Agenbag, J. J. and Duncombe Rae, C. M. (1998). An upwelling filament north-west of Cape Town, South Africa. Afr. J. Marine Sci., 19(1), 75-88, doi: 10.2989/025776198784126953.

Olson, D. B. and Evans, R. H. (1986). Rings of the Agulhas current. Deep Sea Res., Part I, 33(1), 27-42, doi: 10.1016/0198-0149(86)90106-8.

555   Peña-Molino, B., Joyce, T. M. and Toole, J. M. (2012). Variability in the deep western boundary current: Local versus remote forcing. J. Geophys. Res., 117(C12), doi: 10.1029/2012JC008369.

Perez, R. C., Garzoli, S. L., Meinen, C. S. and Matano, R. P. (2011). Geostrophic velocity measurement techniques for the meridional overturning circulation and meridional heat transport in the South Atlantic. J. Atmos. Oceanic Technol., 28(11), 1504-1521, doi: 10.1175/JTECH-D-11-00058.1.

Ocean Science
Discussions

Open Access

EGU

560   Piollé, J.-F. and Autret, E. (2011). Product user manual for ODYSSEA level 3 and 4 global and regional products, Proj. FP7-SPACE-2007-1, Ifremer, Issy-les-Moulineaux, France. Available at: http://projets.ifremer.fr/cersat/Data/Discovery/By-parameter/Sea-surface-temperature/ODYSSEA-Global-SST-Analysis.

Pujol, M. I., Faugère, Y., Taburet, G., Dupuy, S., Pelloquin, C., Ablain, M. and Picot, N. (2016). DUACS DT2014: the new multi-mission altimeter data set reprocessed over 20 years. Ocean Sci., 12(5), 1067-1090, doi: 10.5194/os-12-1067-2016.

565   Rahmstorf, S., Feulner, G., Mann, M. E., Robinson, A., Rutherford, S. and Schaffernicht, E. J. (2015). Exceptional twentieth-century slowdown in Atlantic Ocean overturning circulation. Nat. Clim. Change, 5(5), 475-480, doi: 10.1038/nclimate2554.

Richardson, P. L., Lutjeharms, J. R. E. and Boebel, O. (2003). Introduction to the "Inter-ocean exchange around southern Africa". Deep Sea Res., Part I, 50(1), 1-12, doi: 10.1016/S0967-0645(02)00376-4.

Roemmich, D. and Cornuelle, B. (1992). The subtropical mode waters of the South Pacific Ocean. J. Phys. Oceano., 22(10), 570   1178-1187, doi: 10.1175/1520-0485(1992)022<1178:TSMWOT>2.0.CO;2.

Rossby, T., Flagg, C. and Donohue, K. (2010). On the variability of Gulf Stream transport from seasonal to decadal timescales. J. Mar. Res., 68(3-1), 503-522, doi: 10.1357/002224010794657128.

de Ruijter, W. P. M., Biastoch, A., Drijfhout, S. S., Lutjeharms, J. R. E., Matano, R. P., Pichevin, T., van Leeuwen, P. J. and Weijer, W. (1999). Indian-Atlantic interocean exchange: Dynamics, estimation and impact. J. Geophys. Res., 104(C9), 575   20885-20910, doi: 10.1029/1998JC900099.

Rusciano, E., Speich, S. and Ollitrault, M. (2012). Interocean exchanges and the spreading of Antarctic Intermediate Water south of Africa. J. Geophys. Res., 117(C10), doi: 10.1029/2012JC008266.

Schiermeier, Q. (2013). Oceans under surveillance. Nature, 497(7448), 167-169.

Schott, F. A., Dengler, M., Zantopp, R., Stramma, L., Fischer, J. and Brandt, P. (2005). The shallow and deep western 580   boundary circulation of the South Atlantic at 5°-11°S. J. Phys. Oceano., 35(11), 2031-2053, doi: 10.1175/JPO2813.1.

Schouten, M. W., de Ruijter, W. P. M., van Leeuwen, P. J. and Lutjeharms, J. R. E. (2000). Translation, decay and splitting of Agulhas rings in the southeastern Atlantic Ocean. J. Geophys. Res., 105(C9), 21913–21925, doi: 10.1029/1999JC000046.

Send, U., Lankhorst, M. and Kanzow, T. (2011). Observation of decadal change in the Atlantic meridional overturning circulation using 10 years of continuous transport data. Geophys. Res. Lett., 38(24), doi: 10.1029/2011GL049801.

585   Speich, S., et al. (2007). GOODHOPE/Southern Ocean: A study and monitoring of the Indotlantic connections. Mercator Newsletter, October 2007, 27, 29–41.

Speich , S., Garzoli, S., Piola, A. and the SAMOC community (2010). A monitoring system for the South Atlantic as a component of the MOC. In Proceedings of OceanObs'09: Sustained Ocean Observations and Information for Society (Annex), Venice, Italy, 21-25 September 2009, Hall, J., Harrison, D.E. & Stammer, D., Eds., ESA Publication WPP-306.

590   Srokosz, M. A. and Bryden, H. L. (2015). Observing the Atlantic Meridional Overturning Circulation yields a decade of inevitable surprises. Science, 348(6241), 1255575, doi: 10.1126/science.1255575.

Thomson, R. E. and Emery, W. J. (2014). Chapter 3 - Statistical Methods and Error Handling, In Data analysis methods in physical oceanography (Third Edition). Elsevier, Boston, 219-311 pp, doi: 10.1016/B978-0-12-387782-6.00003-X.

Valla, D., Piola, A. R., Meinen, C. S. and Campos. E. (under review, 2017). Strong mixing and recirculation in the

595   northwestern Argentine Basin. Under review, JGR Oceans.

Van Aken, H. M., Van Veldhoven, A. K., Veth, C., De Ruijter, W. P. M., Van Leeuwen, P. J., Drijfhout, S. S., Whittle, C. P. and Rouault, M. (2003). Observations of a young Agulhas ring, Astrid, during MARE in March 2000. Deep Sea Res., Part II, 50(1), 167-195, doi: 10.1016/S0967-0645(02)00383-1.

Watts, D. R., Sun, C., & Rintoul, S. (2001). A two-dimensional gravest empirical mode determined from hydrographic

600   observations in the Subantarctic Front. J. Phys. Oceano., 31(8), 2186-2209, doi: 10.1175/1520-0485(2001)031<2186:ATDGEM>2.0.CO;2.

Weijer, W., de Ruijter, W. P., Dijkstra, H. A., and Van Leeuwen, P. J. (1999). Impact of interbasin exchange on the Atlantic overturning circulation. J. Phys. Oceanogr., 29(9), 2266-2284, doi: 10.1175/1520-0485(1999)029<2266:IOIEOT>2.0.CO;2.

Whittle, C., Lutjeharms, J. R. E., Rae, D. and Shillington, F. A. (2008). Interaction of Agulhas filaments with mesoscale

605   turbulence: a case study. S. Afr. J. Sci., 104(3-4), 135-139.

Ocean Science
Discussions

Open Access

EGU
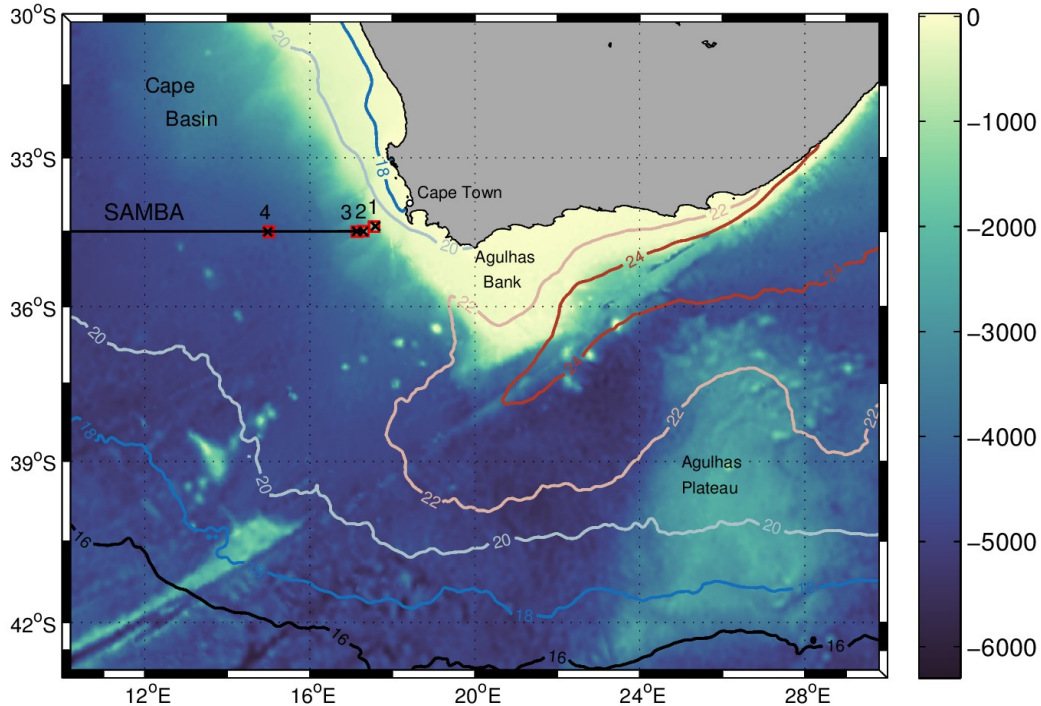
Figure 1: Study area with shaded color representing the bathymetry [m] from Etopo1. The thin black line denotes the position of the SAMBA line and the black crosses (red squares) represent the mooring (CPIES) positions with their associated numbers (1, 2, 3 and 4). 2015 annual averaged SST isotherms from the ODYSSEA dataset are plotted with colored contours.
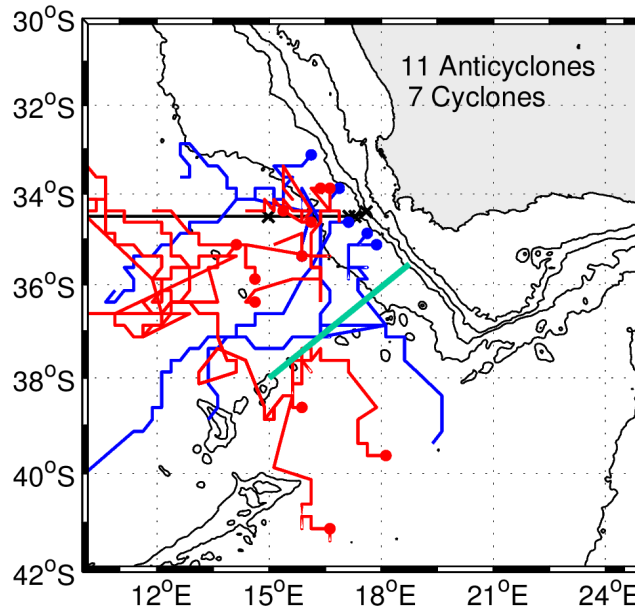

610 **Figure 2: Eddy trajectories from September 15, 2014 to December 15, 2015 for eddies influencing the moorings measurements. The red lines are trajectories of anticyclonic eddies and blue lines trajectories of anticyclonic eddies. The circles indicate the starting positions of an eddy track. The green line represents the northern route of Agulhas rings defined by Dencause et al. (2010).**
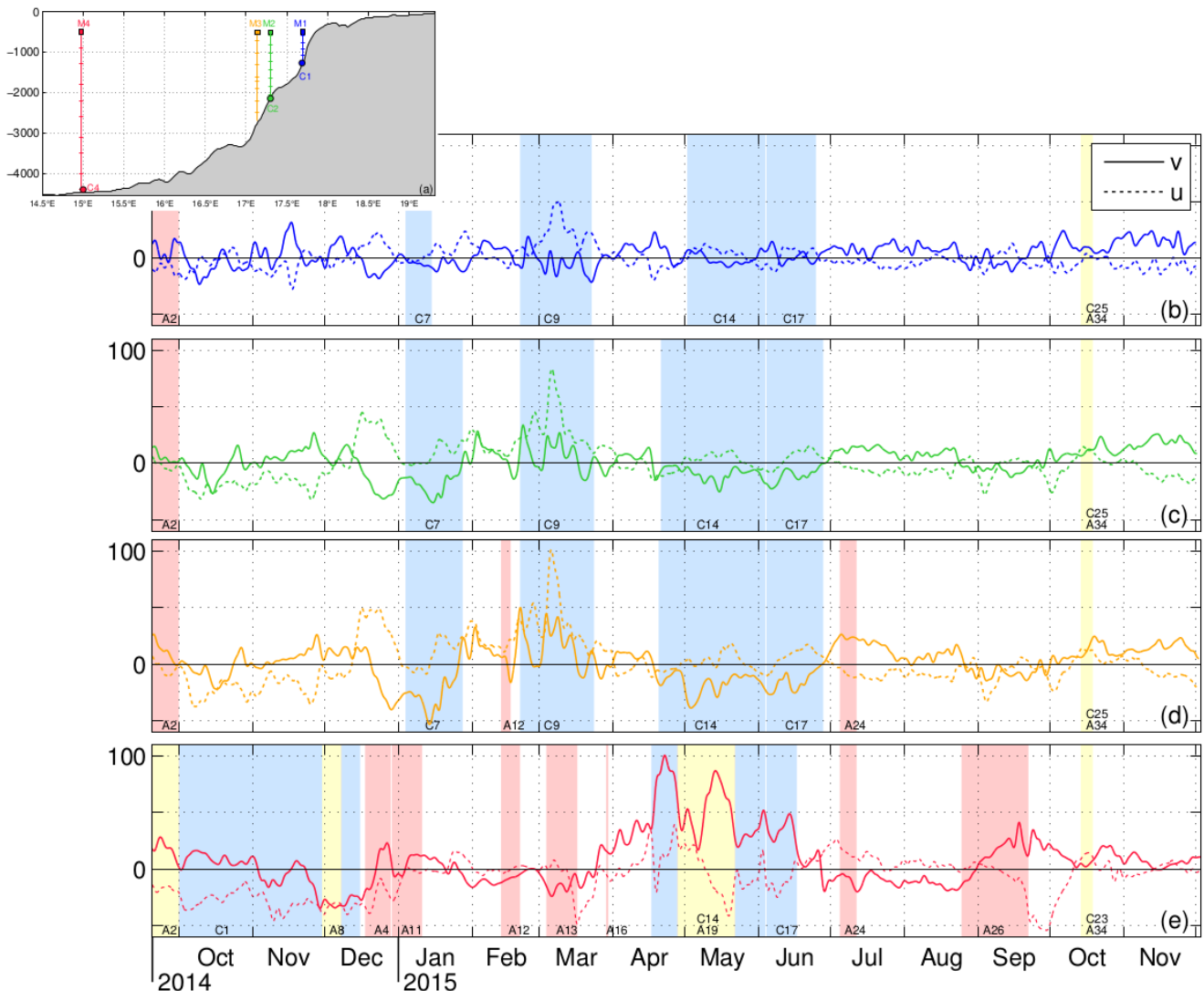
Figure 3: (a) Vertical scheme of the mooring lines positions along the latitude 34.5°S. The squares represent the upward-looking
ADCP positions, the small horizontal lines indicate the SBE Microcat's sensors and the circles at the bottom show the CPIES.
615 Temporal evolution of the depth-averaged u (dashed line) and v (solid line) component of the current velocity at M1 (b - blue line),
M2 (c - green line), M3 (d - blue line) and M4 (e - red line) [cm s^{-1}]. The shaded areas show the eddy events defined with altimetry
data (red: anticyclonic eddies, yellow: dipole events and blue: cyclonic eddies).
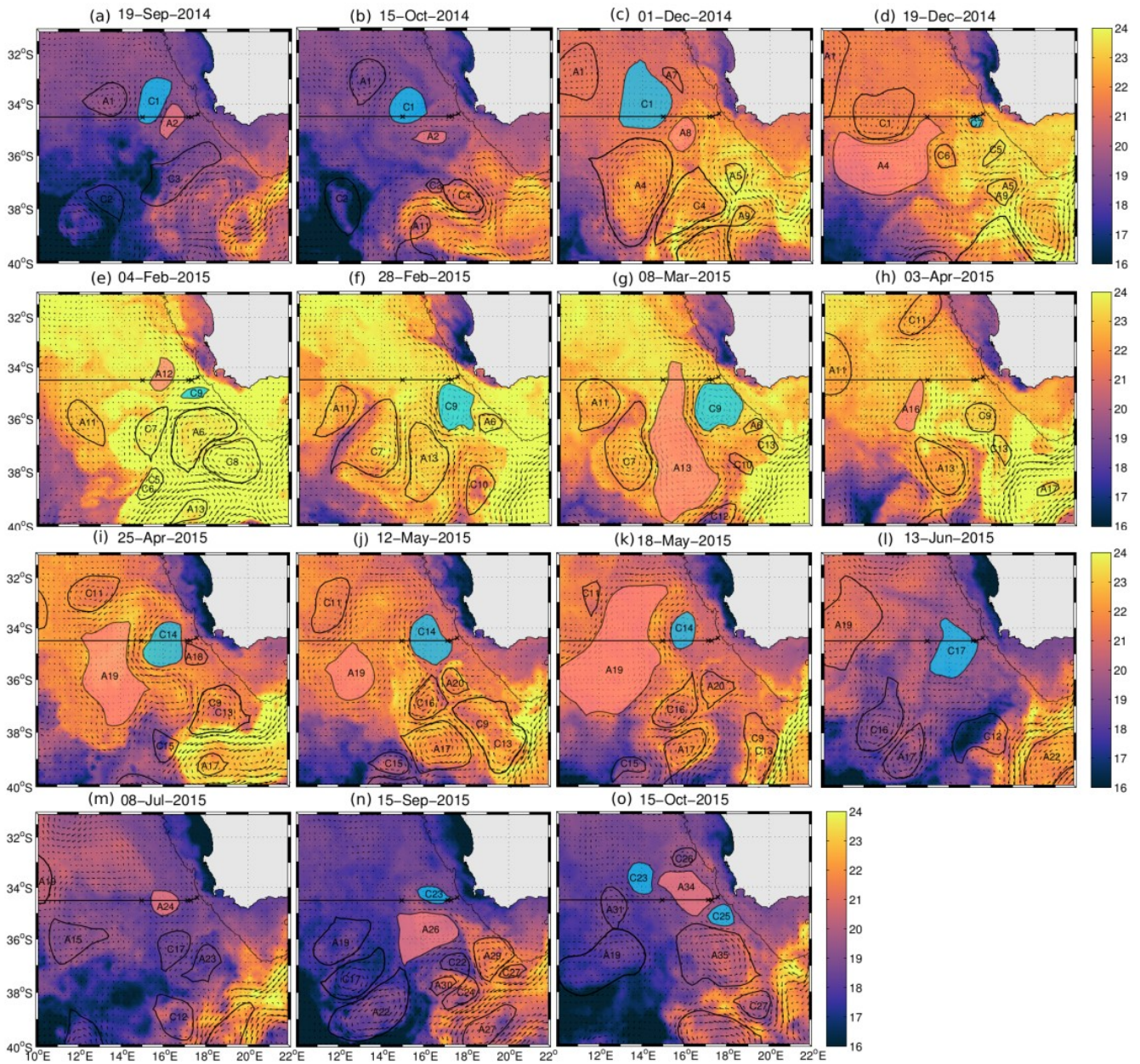
Figure 4: SST satellite images from September 19, 2014 to October 15, 2015. The black line denotes the position of the SAMBA line and the crosses represent the mooring positions. Black contours show the eddies identification named as CN (cyclonic eddies) and AN (anticyclonic eddies), with N a number assigned in chronological order by the eddy tracking scheme. The colored eddies (red for AN and blue for CN) are identified as close enough to affect the measurement at the different moorings.

Ocean Science
Discussions
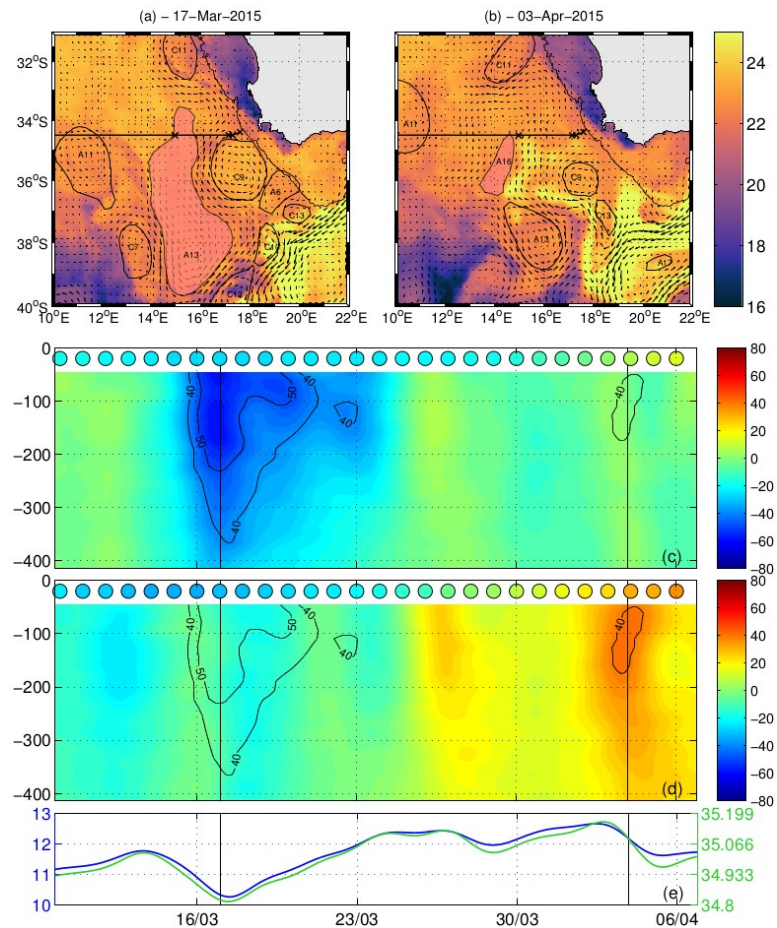
625 **Figure 5: #Anticyclonic eddy: (a, b) SST satellite images for the day of maximum averaged current magnitude recorded at M4 (vertical black lines on the time series). Vertical-temporal section of the u-component (c) and v-component (d) of the current speed measured from the upward-looking ADCP at M4. The current amplitude contours (40 cm s^{-1} and 50 cm s^{-1}) are highlighted on these sections with black contours. The colored circles at the top of the section show the u-component and v-component of the current speed from altimetry data. (e) Temporal evolution of temperature (blue line) and salinity (green line) recorded at the 500**
630 **m depth SBE37 Microcat's.**
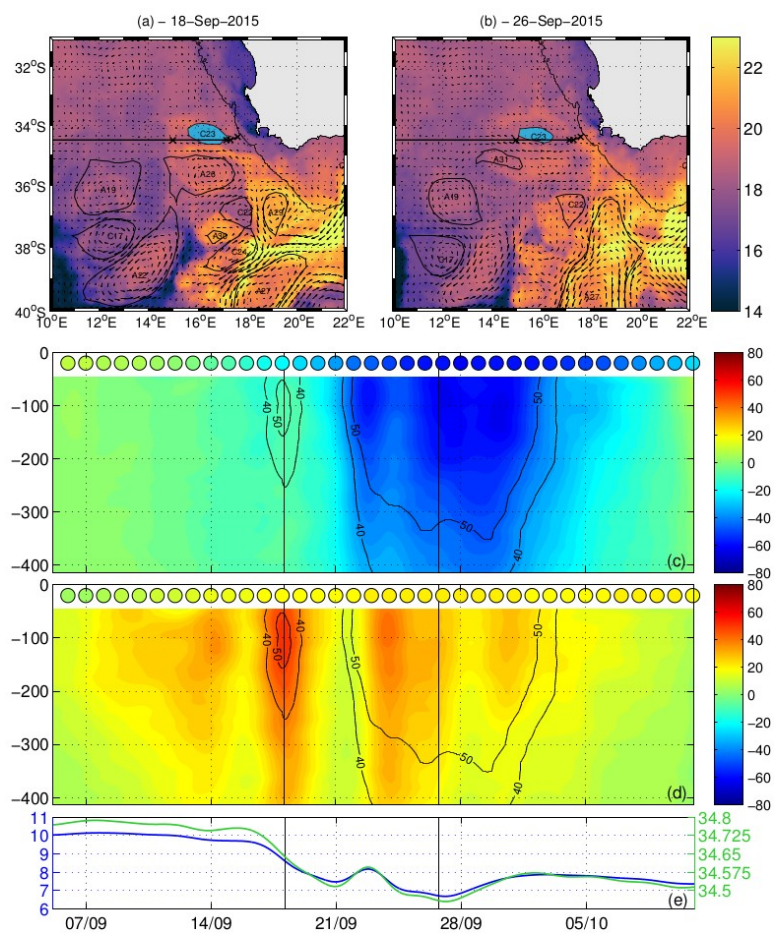
Figure 6: Same as Fig. 5 for #Cyclonic eddy

Ocean Science
Discussions

Open Access

EGU
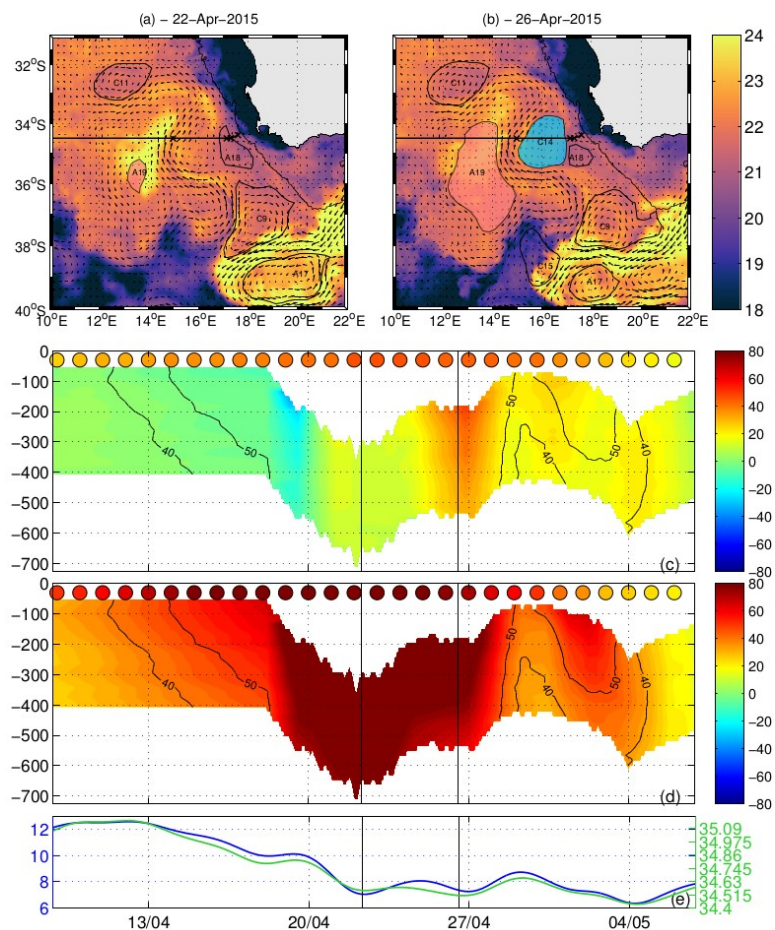
Figure 7: Same as Fig. 5 for #Cold intrusion water

Ocean Science
Discussions
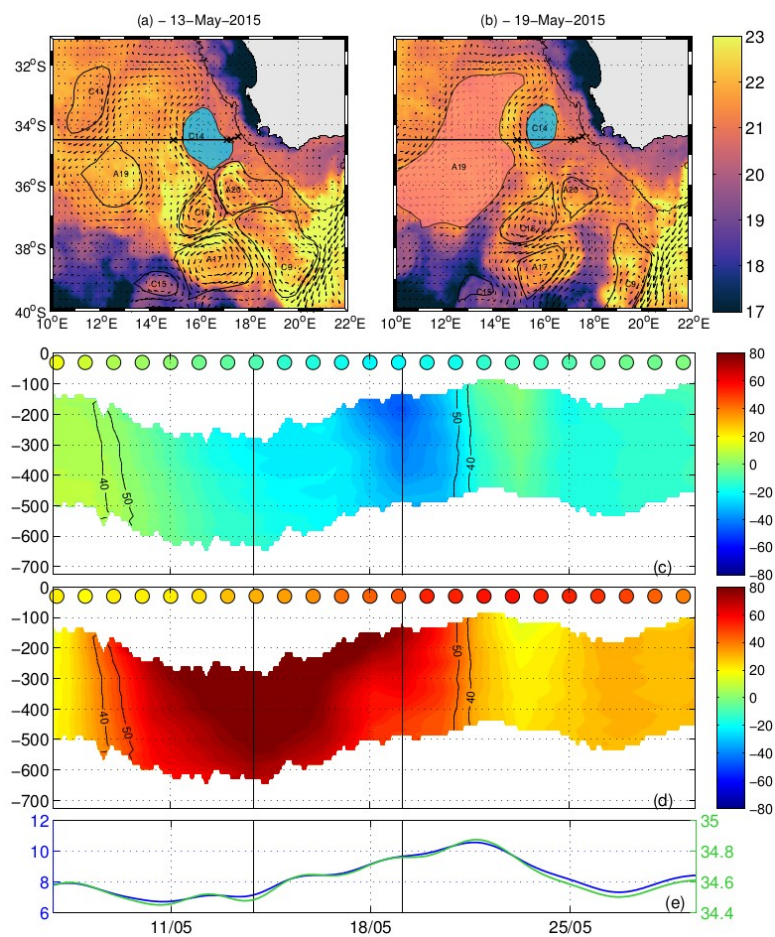
Figure 8: Same as Fig. 5 for #Warm intrusion water

Ocean Science
Discussions
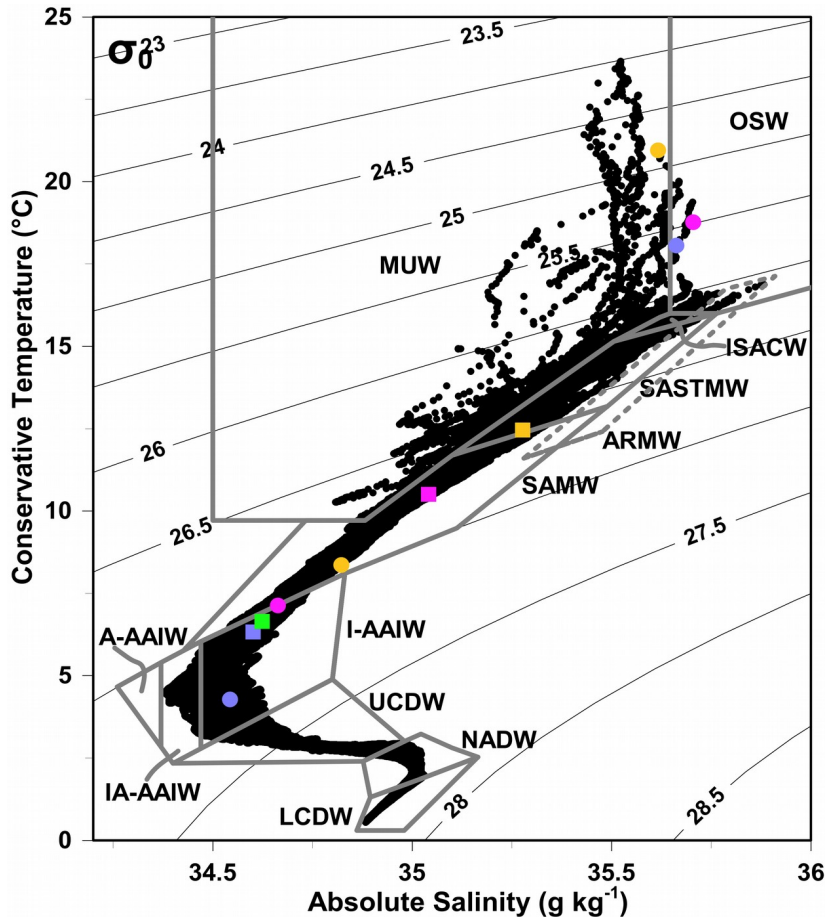
Figure 9: Conservative Temperature (°C) – Absolute Salinity (g kg⁻¹) relationship for the SAMBA transect. Water masses are indicated by gray boxes (OSW – Oceanic Surface Water, MUW – Modified Upwelled Water, lSACW – Light South Atlantic Central Water, SASTMW – South Atlantic Subtropical Mode Water, SAMW – Subantarctic Mode Water, ARMW – Agulhas Ring Mode Water, I-AAIW – Indian Antarctic Intermediate Water, IA-AAIW – Indo-Atlantic Antarctic Intermediate Water, A-AAIW – Atlantic Antarctic Intermediate Water, UCDW – Upper Circumpolar Deep Water, NADW – North Atlantic Deep Water, and LCDW – Lower Circumpolar Deep Water). The colored squares (SBE37 MicroCATs) and circles (reconstructed GEM field) represents the water masses associated to each case studies (#Anticyclonic eddy: yellow, #Cyclonic eddy: green, #Cold intrusion: violet, #Warm intrusion: pink).

Ocean Science

Discussions

Open Access

EGU
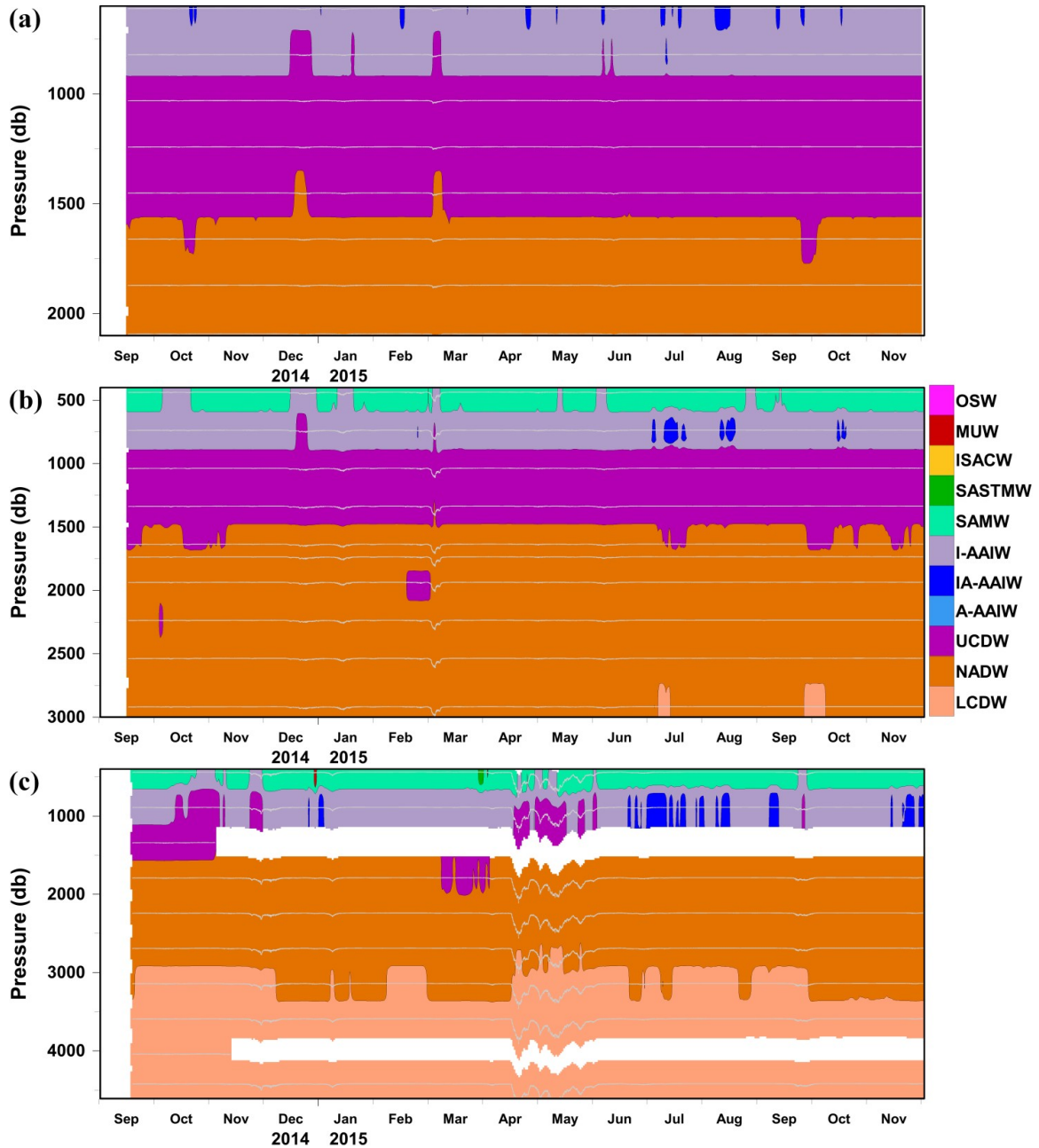
Figure 10: Daily averaged vertical distribution of water masses at moorings (a) M2, (b), M3, and (c) M4, along the SAMBA transect. Grey horizontal lines indicate the locations of SBE37 MicroCATs.

650
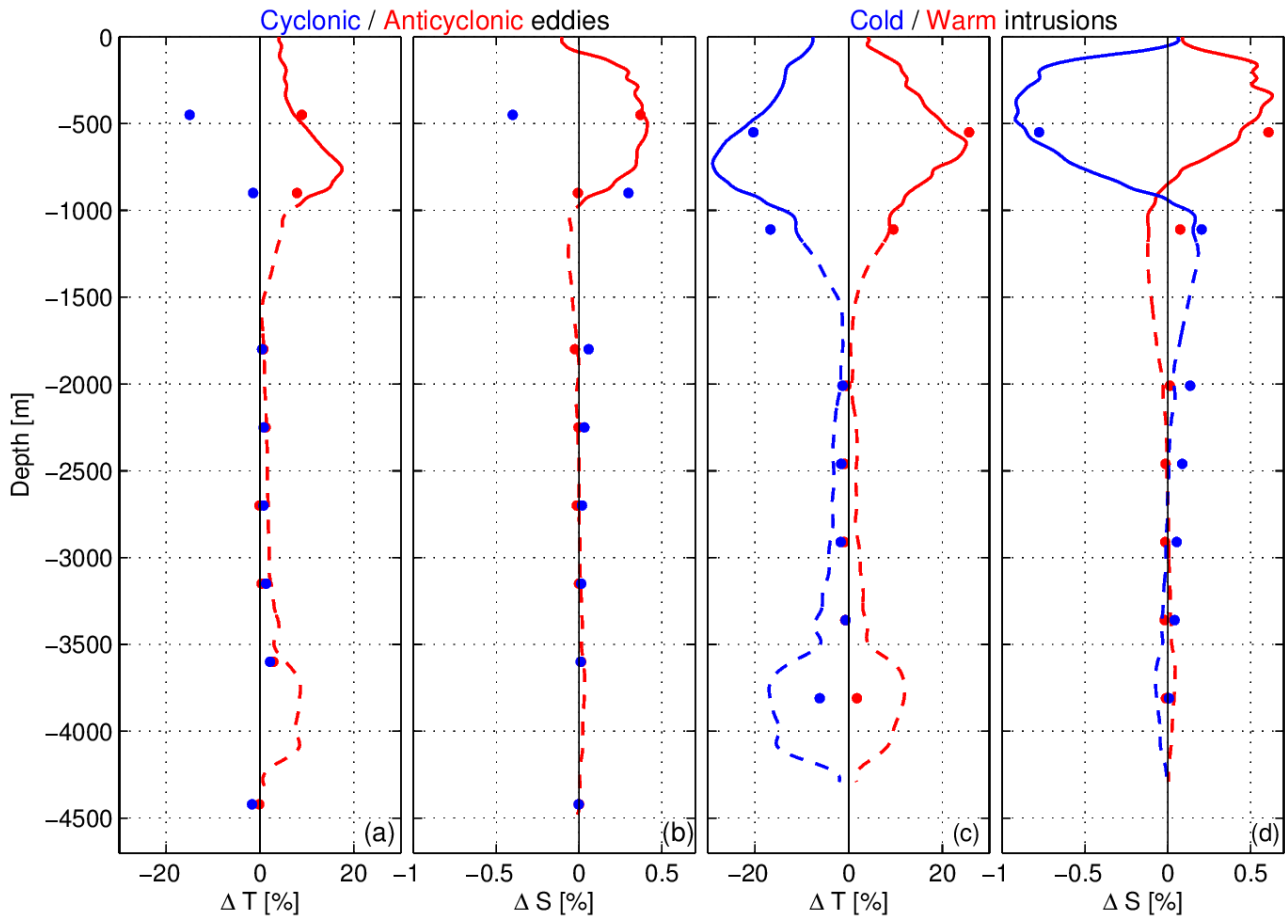
Figure 11: Vertical profiles of the temperature (a,c) and salinity (b,d) percent changes at M4 due to the presence of the #Anticyclonic eddy; #Cyclonic eddy (a,b) and #Cold intrusion water; #Warm intrusion (c,d). The colored dots represent the value from the SBE37 Microcat's and the dashed/solid lines from the reconstructed GEM fields.

Table I: Moorings and CPIES characteristics.

	Lat / Lon	Water depth	Start / End	Instruments (Depth [m])
Mooring 1 - M1	34ºS 23.636' 17ºE 35.664'	1121 m	17/09/2014 08:00 01/12/2015 05:00	75kHZ RDI ADCP (580) SBE 37 SMP (600, 770, 930, 1090)
CPIES 1 - C1	34ºS 24.348' 17ºE 33.456'	1266 m	07/09/2013 00:00 11/08/2015 00:00	
Mooring 2 - M2	34ºS 29.960' 17ºE 18.064'	2094 m	17/09/2014 11:00 01/12/2015 13:00	75kHZ RDI ADCP (590) SBE 37 SMP (605, 810, 1020, 1230, 1435, 1642, 1850, 2070)
CPIES 2 - C2	34ºS 29.813' 17ºE 18.036'	2129 m	07/09/2013 00:00 11/08/2015 00:00	
Mooring 3 - M3	34ºS 30.010' 17ºE 8.3640	2970 m	17/09/2014 16:00 02/12/2015 10:00	75kHZ RDI ADCP (410) SBE 37 SMP (435, 730, 1030,1325, 1620, 1720, 1915, 2210, 2505, 2880)
CPIES 3 - C3	34ºS 29.964' 17ºE 8.3100'	2850 m	No data	
Mooring 4 - M4	34ºS 30.360' 14ºE 58.810'	4474 m	19/09/2014 23:00 03/12/2015 05:00	75kHZ RDI ADCP (415) SBE 37 SMP (450, 895, 1340, 1780, 2250, 2665, 3110, 3550, 3985, 4360)
CPIES 4 - C4	34ºS 30.252' 15ºE 0.161'	4482 m	07/09/2013 00:00 11/08/2015 00:00	

Table II: Summary of comparison statistics for satellite altimetry and moored current meter, with R the correlation coefficient, ΔV_{rms} the root mean square differences between the zonal and meridional components of ADCPs and those from altimetry (Eq. 1), and the bias between those components (Eq. 2).

	R		ΔV_{rms} [cm s^{-1}]		Bias [cm s^{-1}]	
	u	v	u	v	u	v
M1 (54.9 m)	0.32	0.30	15.4	13.3	5.3	-1.5
M2 (60.7 m)	0.72	0.59	14.0	12.9	3.0	-8.8
M3 (43.0 m)	0.81	0.67	13.3	13.9	-5.8	1.2
M4 (45.8 m)	0.80	0.83	13.0	15.9	-4.3	-4.9

Ocean Science
Discussions

Open Access

EGU

Table III: Characteristics of the eddies affecting the moorings data detected by satellite altimetry. The time period and the radius of the different eddies are derived from the eddy detection method. The velocity magnitude maxima recorded at the upward-looking ADCP mooring are also indicated. The eddies are named as CN (cyclonic eddies) and AN (anticyclonic eddies), with N a number assigned in chronological order by the eddy tracking scheme. Agulhas rings are identified with a star.

Time Beg Time End Radius [km] max(V_{adcp}) [cm s^{-1}]	A2*	A4*	A8*	A11*	A12	A13*	A16*	A19*	A24	A26*	A34
M1											
M2											
M3	09/20/14 10/01/14 117.2 33.4				02/13/15 02/17/15 103.6 12.4				07/05/15 07/12/15 58.1 22.4		10/14/15 10/19/15 95.9 17.3
M4		12/18/14 12/29/14 169.9 43.2	11/30/14 12/08/14 59.6 50.5	12/18/14 01/11/15 139.0 28.5	02/13/15 02/21/15 97.8 12.5	03/04/15 03/17/15 148.2 49.5	03/29/15 03/30/15 71.7 16.8	04/28/15 05/22/15 153.4 89.0		08/25/15 09/22/15 112.4 42.0	

Time Beg Time End Radius (km) max(V_{adcp}) [cm s^{-1}]	C1	C7	C9	C14	C17	C23	C25
M1		01/04/15 01/15/15 56.6 9.8	02/21/15 03/23/15 91.0 104.3	05/02/15 06/04/15 82.8 13.3	06/05/15 06/25/15 85.0 18.2		10/14/15 10/19/15 51.3 26.7
M2		01/04/15 01/28/15 56.2 53.4		04/21/15 06/04/15 84.6 38.9	06/05/15 06/28/15 86.0 28.3		
M3							
M4	09/05/14 12/16/14 97.5 50.7			04/17/15 06/04/15 83.3 101.1	06/04/15 06/17/15 77.0 50.2	10/14/15 10/19/15 70.0 14.7	

665